New constraints on biological production and mixing processes in the South China Sea from triple isotope composition of dissolved oxygen

Hana Jurikova[1], Osamu Abe[2], Fuh-Kwo Shiah[3], and Mao-Chang Liang[4]

[1]School of Earth and Environmental Sciences, University of St Andrews, KY16 9AL St Andrews, United Kingdom
[2]Graduate School of Environmental Studies, Nagoya University, 464-8601 Nagoya, Japan
[3]Research Center for Environmental Changes, Academia Sinica, 11529 Taipei, Taiwan
[4]Institute of Earth Sciences, Academia Sinica, 11529 Taipei, Taiwan

Correspondence to: Hana Jurikova (hj43@st-andrews.ac.uk) and Mao-Chang Liang (mcl@gate.sinica.edu.tw)

Abstract. South China Sea (SCS), world's largest marginal sea, plays an important role in the global as well as regional biogeochemical cycling of carbon and oxygen. However, its overall metabolic balance, primary production rates, and their link to East Asian Monsoon forcing still remain poorly constrained. Here, we report seasonal trends in triple oxygen isotope composition ($^{17}\Delta$) of dissolved O_2, a tracer for biological O_2, gross primary production (GP; inferred from $\delta^{17}O$ and $\delta^{18}O$ values), and net community production (NP; evaluated from oxygen–argon ratios) from the SouthEast Asian Time-series Study (SEATS) in SCS. Our results suggest stable mixed-layer GP rates of 1.8 g C m^{-2} d^{-1} and NP of -0.02 g C m^{-2} d^{-1} during the summer southwest monsoon, indicating the prevalence of net heterotrophy. During winter months characterised by stronger northeast monsoon forcing, the system is more dynamic with variable production rates, which may shift the metabolism from net heterotrophy to net autotrophy (NP up to ~0.15 g C m^{-2} d^{-1}). These findings underscore the importance of monsoon intensity on tilting the carbon balance from source to sink in a warm oligotrophic sea, and on driving the regional circulation pattern. Finally, our data from the deeper regions show that SCS circulation is strongly affected by monsoon wind forcing, with a larger part of the water column down to at least 400 m depth fully exchanged during a winter, suggesting the $^{17}\Delta$ of deep O_2 as a valuable novel conservative tracer for probing mixing processes from a new perspective.

1 Introduction

The South China Sea (SCS) represents the largest marginal sea of the world, influencing the regional as well as global biogeochemical cycling of carbon and oxygen. It has been suggested that marginal seas as a whole may act as a significant global atmospheric carbon dioxide sink, primarily due to CO_2 absorption by continental shelf waters (Tsunogai et al., 1999; Liu et al., 2000; Yool and Fasham, 2001; Chen et al., 2003; Thomas et al., 2004). However, the heterogeneous nature together with latitudinal differences between ocean margins makes any joint extrapolations to a global scale unrepresentative. Most observation have revealed that, in particular seas at mid-latitude shelves, which experience strong spring blooms and clear seasonal patterns, function as CO_2 sinks (e.g. the North Sea (Frankignoulle and Borges, 2001); the

Gulf of Biscay (Thomas et al., 2004); the Celtic Sea (Seguro et al., 2019); the East China Sea (Tsunogai et al., 1999; Wang et al., 2000) or the Middle Atlantic Bight (DeGrandpre et al., 2002)). The tropical and subtropical shelves and marginal seas, on the other hand, are most likely CO_2 sources, due to the high annual surface temperature and the absence of strong spring blooms (Cai and Dai, 2004). Similar scenario may also be anticipated for the SCS. While several studies reaffirmed that the

35   SCS indeed acts as a source of CO_2 to the atmosphere in the spring, summer and autumn (Rehder and Suess, 2001; Zhai et al., 2005), Tseng et al. (2005) reported on the uptake of CO_2 during winter from SCS. The observed CO_2 invasion, driven by an unusual seasonal pattern in phytoplankton biomass in the oligotrophic open northern part during winter, was apparently large enough to compensate for the CO_2 evasion during the rest of the year, resulting in only minor net annual sea–atmosphere CO_2 fluxes (Tseng et al., 2005). Clearly, the role of the SCS, and marginal seas in general, is complex and their

40   seasonal carbon cycling needs to be further examined. This presents an even more pressing challenge under the current on-going climatic changes, and will be critical for improving our future CO_2 projections and climate models.

Owing to its position between the Tibetan Plateau and the western Pacific warm pool, SCS is continuously exposed to the East Asian Monsoon, which plays a fundamental role in the oceanography and biogeochemistry of the SCS (see Wong et al.,

45   2007 for an overview). From June to September, the weaker southwest summer monsoon (SWM) drives the anti-cyclonic circulation gyre; while between November and April the strong northeast winter monsoon (NEM) propels a basin-wide cyclonic circulation gyre (Fig. 1). This intense seasonal reversal drives the short- and long-term physical, chemical and biological processes that control the distribution patterns of phytoplankton communities (Ning et al., 2004). As a result, medium chlorophyll a (Chl−a) concentrations are typically associated with the SWM, while highest productivity is expected

50   during the NEM due to increased diapycnal nutrient supply from the thermocline (Liu et al., 2002; Li et al., 2017). Lowest Chl−a have been observed during inter-monsoon seasons (Wong et al., 2007).

Accurate quantification of phytoplankton production rates, a fundamental property of the ocean system, however, remains a challenge, principally due to methodological biases. This has been a subject of increasing debate over the past years resulting

55   in augmented efforts to compare and resolve production rates through different methods (e.g. Juranek and Quay, 2013; Regaudie-de-Gioux et al., 2014). Alone in the SCS and at the SouthEast Asian Time-series Study (SEATS) our understanding of primary production is predominantly limited to opportunistic assessments using the ^{14}C-assimilation method (Liu et al., 2002) or satellite-based SeaWiFS observations (Liu et al., 2002; Lin et al., 2003). While the traditional ^{14}C approach (Steeman-Nielsen, 1952) is limited due to its in vitro nature, which cannot reflect the time-averaged mixed-

60   layer phytoplankton production (Marra, 2002), the later relies on calibrations against field measurements that are spatially and temporally scarce (Carr et al., 2006). Although not exempt of uncertainties (Juranek and Quay, 2013), as these are inherent to any productivity determination, the triple oxygen isotope composition technique ([17]Δ; Luz et al., 1999; Luz and Barkan, 2000) combined with O_2/Ar measurements has proved to be a powerful tool providing us a new perspective on evaluating primary production (e.g. Sarma et al., 2005; Reuer et al., 2007; Stanley et al., 2010; Hamme et al., 2012; Castro-

65   Morales et al., 2013; Jurikova et al., 2016). The key advantage of this technique is that $^{17}\Delta$ allows for distinguishing photosynthetic O_2 input from other sources directly in situ, while the co-variation of $\delta^{17}O$ and $\delta^{18}O$, the dual-delta approach (Prokopenko et al., 2011; Kaiser, 2011), enables a more exact assessment of integrated gross productivity in the mixed layer.

In order to evaluate the photosynthetic O2 production, carbon balance, and expand our overall understanding of primary
70   production and its link to monsoon forcing in the SCS, we performed triple isotopic analyses of dissolved O_2 ($^{17}\Delta$) from five seasonal vertical profiles at SEATS. The profiles represent summer SMW and winter NEM as well as inter-monsoon conditions. In addition, owing to the conservative behaviour of $^{17}\Delta$ in a parcel of deep water, we use the deep samples to further review the potential of this tracer for assessing mixing processes from a new perspective.

2 Methods

75   ### 2.1 Sampling and analysis

Sampling was carried out aboard R/V OR-1 during cruises CR1053 (in October 2013), CR1084 (August 2014) and CR1103 (April 2015) at station 55 "SEATS" (the SouthEast Asian Time-series Study, 18° N, 116° E, Fig. 1) in South China Sea (SCS). Seawater was collected using rosette sampler equipped with 20-L Niskin bottles attached to a Seabird SBE 911 Plus CTD. Samples for dissolved oxygen analysis were obtained on October 16th in 2013 (11 depths: 5, 10, 30, 50, 80, 100, 150,
80   200, 300, 400 and 500 m), August 5th (11 depths: 5, 10, 20, 80, 100, 200, 600, 1000, 1800, 2500 and 3500 m) and 6th in 2014 (13 depths: 5, 10, 20, 50, 80, 200, 400, 600, 1000, 1200, 1800, 2500 and 3500 m), and on April 24th (14 depths: 5, 10, 20, 80, 100, 150, 200, 300, 400, 500, 600, 1000, 1800 and 3500 m) and April 25th in 2015 (7 depths: 5, 10, 20, 30, 50, 80, 100; see also Supplement).

85   The accuracy of dissolved oxygen concentration measurements from the CTD was verified against in vitro measurements. Briefly, water samples were siphoned into triplicate 60 ml bottles (Wheaton) and Winkler titration method of Pai et al. (1993) was adopted for in vitro dissolved O_2 determination with a precision of 0.2 % r.s.d. (full scale). Mixed layer was defined by 1 °C (ΔT) threshold from temperature at 10 m depth, and further verified by visual inspection of vertical temperature, density and dissolved oxygen profiles. Limit of the photic zone was defined as the depth where the
90   photosynthetically active radiation (PAR) was 1 % of the surface value. We used Ocean Data View (ODV; Schlitzer, 2020) for profile visualisation.

Triple oxygen isotope analyses were carried out at Academia Sinica, Taiwan. The laboratory protocols for dissolved oxygen sample preparation and analysis are detailed in Jurikova et al. (2016). For comparison, selected sample duplicates obtained
95   from the cruise in October 2013 were also measured at Nagoya University, Japan following the protocols previously

described in Sarma et al. (2005). Note that O_2–Ar data is not available for the October 2013 profile due to the setting of gas chromatograph condition at dry ice-acetone slush temperature for complete separation of O_2.

In summary, dissolved gases were extracted from water following Emerson et al. (1995) and Luz et al. (2002). $\delta^{17}O$ and $\delta^{18}O$

100 in O_2 from the purified oxygen-argon mixture were determined by dual inlet mass spectrometry (Thermo Scientific Finnigan MAT 253 IRMS). The triple oxygen isotope composition, or ^{17}O-excess (Luz et al., 1999; Luz and Barkan, 2000) is defined as:

$$[\ln(1 + \delta^{17}O) - \lambda \times \ln(1 + \delta^{18}O)], \tag{1}$$

105

where the isotopic compositions $\delta^{17}O$ and $\delta^{18}O$ represent the deviation of the abundance ratio of an isotopic and normal species in a sample relative to that of a standard:

$$\delta^{*}O = \left[(^{*}O/^{16}O)_{sample}/(^{*}O/^{16}O)_{standard} - 1 \right], \tag{2}$$

110

where $^{*}O$ is either ^{17}O or ^{18}O. Here, $\delta^{17}O$ and $\delta^{18}O$ are expressed with respect to atmospheric air O_2, and following Luz and Barkan (2005) the factor λ is taken to be 0.518. We note that as suggested by Luz and Barkan (2011) a slope of $\lambda = 0.516$ might present a more appropriate choice, however, in order to enable a direct comparison to other studies we prefer the earlier value, which has been largely applied in studies on marine production. The use of a slope $\lambda = 0.516$ would result in a

115 minor only increase in $^{17}\Delta$ (about 1–8 % of the reported values), which for most of the samples remains within the analytical uncertainties.

Our actual and long-term precision (1σ, standard deviation) established from routine measurements (n = 36) of atmospheric air O_2 for $\delta^{17}O$, $\delta^{18}O$, and $^{17}\Delta$ is 0.017 ‰, 0.030 ‰, and 6 per meg, respectively, and our O_2 scale (Jurikova et al., 2016;

120 Liang and Mahata, 2015; Liang et al., 2017) is in agreement with that of Luz and Barkan (2011). The O_2/Ar ratio was obtained by peak jumping following Barkan and Luz (2003), and is expressed as $\delta(O_2/Ar)$ (‰) = $[(32/40)_{sample}/(32/40)_{standard}$ $- 1] \times 10^3$. The long-term precision (1σ) of routine measurements of atmospheric air was better than 5 ‰. The reproducibility (1σ) for the analysis of equilibrated water samples (n = 3) was 0.020 ‰, 0.037 ‰, and 3 per meg for $\delta^{17}O$, $\delta^{18}O$, and $^{17}\Delta$, respectively and 4.6 ‰ for $\delta(O_2/Ar)$; see Jurikova et al. (2016) for further details. c

125 **2.2 Primary production calculations**

To quantify gross production rates from $\delta^{17}O$ and $\delta^{18}O$ values we followed the standard "dual-delta approach" following Prokopenko et al. (2011) and Kaiser (2011), where the gross oxygen production may be calculated as follows:

$$GOP = KC_o \left[\frac{\left(1 - \frac{1+\delta^{17}O_{eq}}{1+\delta^{17}O} \right) - 0.518 \left(1 - \frac{1+\delta^{18}O_{eq}}{1+\delta^{18}O} \right)}{\left(\frac{1+\delta^{17}O_p}{1+\delta^{17}O} - 1 \right) - 0.518 \left(\frac{1+\delta^{18}O_p}{1+\delta^{18}O} - 1 \right)} \right], \qquad (3)$$

130

where δ^*O is the measured value in a sample, δ^*O_{eq} is the air-water equilibrium (Jurikova et al., 2016), and δ^*O_p represents the photosynthetic O2 (Luz and Barkan, 2011). C_o is the O_2 concentration at saturation using solubility coefficients from Benson and Krause (1984) and K is piston velocity, the coefficient for gas exchange (Wanninkhof et al., 2009). K was derived from wind speeds measured on the ship using an anemometer and verified against NCEP data (Fig. 2). Considering

135   the high wind speeds in SCS during the cruises, K was calculated following Ho et al. (2006), and averaged over the O_2 residence time in the mixed-layer preceding sampling (16, 7, and 4 days for October 2013, August 2014 and April 2015, respectively), based on the mixed-layer depth and gas transfer coefficient. Mixed-layer O_2 production time was estimated from measured O_2 concentrations and GOP data, and was generally lower than O_2 residence time (0.5 days for October 2013, 1.5 and 1.0 days for April 5th and 6th 2014, respectively, and 1.0 and 3.6 days for April 24th and 25th 2015, respectively).

140

To assess the net production rates (NOP) we have used the O2/Ar measurements, following the biological O_2 supersaturation concept for net photosynthetic production. Because the physical properties of O_2 and Ar are similar, and Ar has no biological sources and sinks, measurements of Ar concentration in water may be used to remove physical contributions to O_2 supersaturation. The biological oxygen supersaturation $\Delta(O_2/Ar)$ is defined as the relative deviation of the O2/Ar in a sample

145   to the O2/Ar at equilibrium (given in %) with the atmosphere (e.g. Craig and Hayward, 1987; Emerson et al., 1995; Kaiser et al., 2005) and may be calculated as follows:

$$\Delta(O_2/Ar) = \left[\frac{1+\delta(O_2/Ar)_{sample}}{1+\delta(O_2/Ar)_{eq}} - 1 \right], \qquad (4)$$

150   Assuming the mixed layer is at steady state, NOP can be calculated following Luz et al. (2002):

$$NOP = K \times C_o \times [\Delta(O_2/Ar)]. \qquad (5)$$

Production rates were converted from O_2 to C units following the standard approach (e.g., Hendricks et al., 2014; Juranek et

155   al., 2012). To scale GOP to gross C production, we account for the fraction of O_2 linked to Mehler reaction and photorespiration following Laws et al. (2000) by applying a photosynthetic quotient (PQ) of 1.2. For NOP conversion we use a PQ of 1.4 for new production (Laws, 1991).

3 Results

3.1 Oceanographic setting

160   In contrast to the typical features of tropical waters, characterized by minimal seasonal variations, and comparing to the low-latitude Hawaii Ocean Time-series (HOT) station (Karl et al., 1996), the SEATS station located at an even lower latitude is characterised by a distinct phytoplankton biomass and primary production pattern (Tseng et al., 2005; Wong et al., 2007), largely governed by the East Asian Monsoon which plays a key role in the oceanography and biogeochemistry of the SCS (Chao et al., 1996a; Liu et al., 2002). To assess the role of the monsoon forcing on biological production we collected

165   samples during the typical monsoon seasons: the inter-monsoon period in October 2013, the summer southwest monsoon (SWM) in April 2014, and the winter northeast monsoon (NEM) in April 2015. The basin-wide prevailing monsoon forcing coinciding with our sampling period is also evident from the surface wind maps (Fig. 2).

Shallow mixed layer and persistent stratification throughout the year are characteristic features of SEATS. Overall, the

170   mixed layer temperature variations were only minor and depended on the month (Fig. 3). Highest surface temperatures of 29 °C were recorded in the summer in August 2014 (Fig. 3b). In October 2013 (Fig. 3a) the average temperature was 28 °C, and the lowest values of 27 °C were observed towards the end of the winter monsoon in April 2015 (Fig. 3c). Conversely, mixed layer was deepest in October 2013 at 49 m. In August 2014 mixed layer was situated at 31 m and the shallowest mixed layer of 23 m was recorded in April 2015 (Table 1, Fig. 3).

175

Chlorophyll fluorescence was generally low and restricted to the thermocline 50−100 m depths (Fig. 4). Nevertheless, we observed relatively marked seasonal variations. Interestingly, Chl−a was highest of 0.6 mg m^{-3} in October 2013 during the inter-monsoon period (Fig. 4a). In August 2014, during the summer SWM, the concentration remained at 0.2−0.3 mg m^{-3} without pronounced variations and diurnal trends (Fig. 4b). For the winter NEM season we observed again a minor increase

180   in the subsurface chlorophyll maximum, but mostly restricted to the dawn hours of up to 0.5 mg m^{-3} (April 25th, 2015), which gradually declined throughout the day and was lowest at night of approximately 0.2 mg m^{-3} (Fig. 4c).

3.2 Dissolved O_2 composition: $^{17}\Delta$ and $\Delta(O_2/Ar)$

The triple isotope composition of dissolved O_2 profiles from SEATS is shown in Figure 3 and available in Supplement. We observed broad seasonal variations in both the $^{17}\Delta$ and the $\Delta(O_2/Ar)$, with a daily component, overall ranging between 22 and

185   229 per meg and −72 to 2.2 %, respectively. At large, the upper $^{17}\Delta$ profiles outlined a common trend, with low $^{17}\Delta$ in the mixed layer, a peak in the values below, and a gradual decrease towards 200 m depth. The mixed layer values, and the depth of the $^{17}\Delta$ maximum peak as well as its magnitude, however, varied considerably between the seasons. In the shallow mixed layer in August 2014 (Fig. 3b) and April 2015 (Fig. 3c), the $^{17}\Delta$ ranged between ~20−70 per meg due to the fast-changing balance between O_2 produced photosynthetically, which increases the $^{17}\Delta$, and that from gaseous exchange with atmospheric

190 O_2, which reduces the $^{17}\Delta$ value. In October 2013, the mixed layer was relatively deep and with high $^{17}\Delta$ values varying between 69 and 122 per meg. The $^{17}\Delta$ gradually increased with depth to a maximum of 182 per meg at 80 m, and then decreased (Fig. 3a). During months with persistent monsoon winds, highest changes in $^{17}\Delta$ and $\Delta(O_2/Ar)$ occurred in the thermocline. On August 5th the $^{17}\Delta$ maximum of 218 per meg was at 100 m. Conversely, in April the $^{17}\Delta$ variations were comparatively subtle, without a prominent sharp peak, and with values between 125 and 140 per meg in the upper 150 to 50

195 m depth. During the winter NEM period 17Δ was rather low at 200 m accompanied by higher $\Delta(O_2/Ar)$ in contrast to the more positive $^{17}\Delta$ recorded during the summer SWM. Below in the deeper regions, $^{17}\Delta$ remained relatively high, with increased $^{17}\Delta$ values at 1000 m in August 2014, and at 800 m in April 2015.

Our seasonal depth profiles from SEATS share some similarities with the tropical oligotrophic HOT station (Juranek and

200 Quay, 2005), albeit with different $^{17}\Delta$ magnitudes. Notably, the $^{17}\Delta$ depth distribution pattern at SEATS was comparable to that at HOT, with a broad summer $^{17}\Delta$ peak (above 200 per meg at 80 and 100 m depth) from August 2014 comparable to that at HOT during the same month (with values above 140 per meat at 120 and 150 m depth), as well as a high peak in October 2013 (above 180 per meg at 80 m) rather similar to that at HOT during October (above 140 per meg at 100 m). In February, the $^{17}\Delta$ values were overall much lower at HOT, reaching the highest values in the deep (above 90 per meg

205 between 150 and 200 m). Possibly, such trends could also be expected for SEATS, in fact our data from April 2015 appears to bear the closest resemblance to it, although a comparison of the same months would be preferable. Lastly, we note that our maximum upper ocean $^{17}\Delta$ values in the euphotic zone at SEATS were 218 per meg at 100 m, as observed on 5th August 2014 (Fig. 3b), much higher than any previously documented upper ocean values, which typically do not exceed ~160 per meg.

210 **4 Discussion**

4.1 Seasonal trends in photosynthetic vs. atmospheric O_2 input in the upper water column

August 2014 – summer southwest monsoon (SWM) season. The combined approach of $^{17}\Delta$ and $\Delta(O_2/Ar)$ composition of dissolved O_2 has been shown to be a valuable tracer for distinguishing biologically mediated O_2 from that supplied by atmospheric air input to the euphotic zone (Luz et al., 1999; Luz and Barkan, 2000). In August 2014, the $^{17}\Delta$ in the mixed

215 layer oscillated daily between ~40−70 per meg, indicating an intermittent alternation between biological and atmospheric O_2 source (Fig. 3b). The photosynthetic activity, is expected to be minimal during this month, as supported by the low fluorescence (Fig. 4b), and may be attributed to the characteristic strong thermal stratification and nutrient depletion during summer months at SEATS (Wong et al., 2017), which is in agreement with past observations (Liu et al., 2002). Strong gas exchange is also inferred from the near-equilibrium $\Delta(O_2/Ar)$ on both sampling dates. In the thermocline $^{17}\Delta$ gradually

220 increased and $\Delta(O_2/Ar)$ decreased with depth in concord until 100 m.

April 2015 – winter north east monsoon (NEM) season. The most obvious feature of these profiles is the overall lower $^{17}\Delta$ and higher $\Delta(O_2/Ar)$ values on the 25th in contrast to the 24th of April in the upper 50 m (Fig. 3c). Close to equilibrium $^{17}\Delta$ (~20 per meg) on the second sampling day indicate increased air-sea gas exchange rates, which drive new primary

225   production as seen by the elevated $\Delta(O_2/Ar)$ of about 2 % in the mixed layer and also by the intensified fluorescence (Fig. 4c). The distribution and concentration of the deep chlorophyll maximum corresponds to characteristic monsoon-forced trends (Liu et al., 2002) and demonstrates the vitality of the thermocline dwelling phytoplankton and the important role of NEM winds on determining the metabolic balance of the system. The overall lower $^{17}\Delta$ and $\Delta(O_2/Ar)$ values in the upper water column observed in April 2015 when compared to August 2014 may illustrate the extent of wind-induced vertical

230   mixing, which could be sufficient to reach the upper limit of the nutricline (e.g. Ning et al., 2004; Tseng et al., 2005) and supply nutrients to the phytoplankton community. Alternatively, between February and April monsoon winds tend to carry minerals and iron rich dust particles from the deserts in Central Asia to the northern SCS and SEATS (Lin et al., 2007; Duce et al., 1991; Fung et al., 2000), which loading could fuel the enhanced biological production. These profiles thus serve as a good example of the local ecosystem interactions and underscore the close dependence of the phytoplankton communities on

235   the NEM forcing.

October 2013 – inter-monsoon season. The $\Delta(O_2/Ar)$ values for this profile are unfortunately not available and we are limited to discussing the changes in dissolved O_2 content in context of $^{17}\Delta$ only. In comparison to the other seasonal profiles, interestingly, this one shows an overall elevated $^{17}\Delta$ in the mixed layer, implying increased biological O_2 production. Values

240   above 120 per meg as measured at 30 and 50 m of depth seem particularly unusual, as any instantaneous increase in photosynthetic $^{17}\Delta$ signal in the mixed layer is expected to be limited due to continuous exchange with atmospheric O_2 and thus averaged against the background signal. It is also unlikely that these samples could have been affected by contamination, as any leak during sampling or preparation would also result in decreased $^{17}\Delta$ signal due to influence from atmospheric O_2. A very likely explanation for the observed high $^{17}\Delta$ would be the rather short O_2 production time (<1 day)

245   against the relatively very long residence time of O_2 in the mixed layer (16 days; see Section 2.2.), suggesting a sustained accumulation of biologically produced O_2. The timing of the high $^{17}\Delta$ values in the mixed layer (Fig. 3a) also coincides with the overall highest observed fluorescence in this study (Fig. 4a), although the Chl−a maximum was situated below the mixed layer and does not fully concur in depth with the $^{17}\Delta$ peak. Potentially, part of the $^{17}\Delta$ signal may also reflect a transient increase in biological O_2 due to upward flux of dissolved O_2 from the Chl−a maximum horizon (Fig. 4d). In such a case the

250     $^{17}\Delta$ and the production would also integrate O_2 from below the mixed layer, and may complicate the application of the steady state model. Nonetheless, if the observed values really reflect integrated O_2 production this would point towards higher production rates during the inter-monsoon periods than previously thought (Wong et al., 2007).

4.2 Primary production rates in South China Sea

Primary production, the synthesis of organic compounds from carbon-containing species is of critical importance to
255 biogeochemical cycling of carbon and oxygen that sustains the marine ecosystem. In a steady-state system we may
distinguish gross (GP) and net production (NP), where the former represents the total C fixed by primary producers and the
latter the C available to the heterotrophic community. The NP thus amounts to the difference between the GP and
community respiration. NP is positive when GP exceeds respiration and the ecosystem exports or stores organic C, while
negative values result when respiration exceeds GP and the ecosystem respires more organic C than was able to produce.
260 These terms are of fundamental interest to ocean studies. However, their quantification is not straightforward, and thus far
only limited information is available globally and especially from SEATS and the SCS.

Our production rates are summarized in Table 1, derived from δ-values of dissolved oxygen using a steady-state mixed layer
oxygen budget model that allows for determining integrated productivity in the mixed layer over the residence time of O_2 (as
265 detailed in Section 2.2). We find minimal changes between the two consecutive sampling days in August 2014, with mean
GP about 1.8 g C m^{-2} d^{-1}, and low negative NP rates averaging −0.02 g C m^{-2} d^{-1} indicating overall net heterotrophy, which
likely prevails during the summer SWM season. The highly comparable daily trends suggest that the calculated rates might
be a representative estimate for the summer period, as with the exception of sporadic typhoon events, the environmental
conditions are expected to remain rather stable and the water column strongly stratified. Conversely, production was more
270 variable in April 2015, yielding GP of approximately 2.3 g C m^{-2} d−1 and NP of −0.16 g C m^{-2} d^{-1} on the first day, and 0.7 g
C m^{-2} d^{-1} and 0.15 g C m^{-2} d^{-1} on the second day, respectively. This points towards a more dynamic system during the
winter NEM period that may shift from net heterotrophy to net autotrophy, due to cooler temperatures and wind-induced
mixing. Highest GP estimates were obtained in October 2013 of 5.9 g C m^{-2} d^{-1}, which is rather surprising since during
inter-monsoon periods phytoplankton production is expected to be limited. The origin of the high GP rates in October 2013
275 appears related to the deep mixed layer with elevated $^{17}\Delta$ values (>120 per meg) measured at 30 and 50 m. These estimates,
however, should not be taken at a face value as diapycnal mixing across the base of the mixed layer, and/or heterogenous
distribution of phytoplankton in the water column and potential in situ production at depth cannot be ruled out in which case
the steady state no longer applies.

Furthermore, we note that the calculated production rates should be considered as minimum production only. At SEATS the
281 euphotic zone was persistently deeper than the mixed layer during our sampling (Fig. 3), which may lead to an
underestimation of the rates, since the share of the production that takes place within the euphotic zone below the mixed
layer cannot be accounted for by the present model. Nonetheless, it is likely that if the respiration exceeds gross production
in the mixed layer, and hence the NP is negative, the overall NP in the euphotic zone will also be negative, since deeper
285 regions tend to have higher respiration rates. Thus, production estimates from paired $^{17}\Delta$ and $\Delta(O_2/Ar)$ profiles are still

useful for indicating trends in ecosystem metabolism, even on instances when the depths of the mixed and euphotic layer differ. Our findings indicate that over the year respiration probably exceeds GP, but with the frequency as well as intensity of the NEM forcing likely playing a critical role in determining the overall metabolic balance of the ecosystem. Hence, production during winters with cooler temperatures and windy days may indeed compensate for the overall annual

290 consumption and lead to fixation of organic C. Weakening of the East Asian Monsoon by anthropogenically induced global warming (e.g. Hsu and Chen, 2002; Xu et al., 2006) is, however, likely to limit vertical transport and nutrient supply to the phytoplankton, resulting in prolonged net heterotrophy, adversely affecting the primary production and C balance at SEATS and SCS.

295 Available data based on ^{14}C observations and modelling studies suggests that primary production in the SCS falls within of range of 120–170 g C m^{-2} year^{-1} (Ning et al., 2004; Chen, 2005; Liu et al., 2002). These values reflect the net, euphotic-zone integrated production, making straightforward comparison to our NP data problematic. Nonetheless to put it in context, assuming no seasonality, this translates to roughly 340 to 480 mg C m^{-2} d^{-1}, which is much higher than our NP range (–160 and 152 mg C m^{-2} d^{-1}, Table 1). This is rather unexpected as the in situ approach when compared to the in vitro technique

300 tends to overestimate the production rates (Juranek and Quay, 2005; Quay et al., 2010; Jurikova et al., 2016), since it reflects time averaged rather than instantaneous production as in the case of the in vitro rates. Thus, unless PP rates in SCS have substantially declined over the past decade, or previous measurements were biased by favourable environmental conditions, it appears that our results underestimate the actual rates. This could be explained by the fact that the estimates do not account for production throughout the entire euphotic zone, suggesting that a substantial part of productivity at SEATS takes place

305 below the mixed layer. However, the possibility that the rates simply reflect the natural variability of the system under seasonal and global changes, since observations of PP at SEATS and in the SCS are rather scarce, should not be excluded.

Obviating the estimates from October 2013, our GP and NP rates compare reasonably well to those based on δ-values from HOT, where seasonal variation in GP and NP were in the range of 800–1470 mg C m^{-2} d^{-1} and –120 and 180 mg C m^{-2} d^{-1}

310 (Juranek and Quay, 2005). Generally, we would, however, expect higher rates at SEATS, where both seasonal monsoon forcing and/or episodic typhoon events induce sufficient vertical mixing to bring nutrients to the mixed layer and stimulate primary production. Assuming that our rates present an underestimation of the productivity due to the relatively very shallow mixed layer, these differences could reconcile. Our observed variations in NP/GP (between –0.01 and –0.02 in August 2014, and –0.07 and 0.21 in April 2015) also compare fairly well with the seasonal trends reported from HOT (between –0.13 and

315 0.13 during summer and winter; Juranek and Quay, 2005) with trends toward heterotrophy in the summer and autotrophy during months. Very low ratios (~0.06) were observed from other low latitude regions such as the Equatorial Pacific (Hendricks et al., 2005; Stanley et al., 2010). This supports the general parallels in ecosystem metabolism in the oligotrophic regions, but also, given the broader variations in NP/GP ratios at SEATS, emphasizes the importance of the monsoon forcing on driving dynamics in a system.

4.3 New insights into the $^{17}\Delta$ in deep water

320

The $^{17}\Delta$ has been traditionally applied for evaluating primary production in the upper ocean, and thus far only little is known on the $^{17}\Delta$ composition of the deep ocean. Due to the conservative behaviour of O_2 in a parcel of deep water, where it may no longer be influenced by air–sea gas exchange or photosynthesis, the $^{17}\Delta$ could also present a valuable tracer for deep water mixing processes, since any variations in $^{17}\Delta$ can only result from mixing of waters with different $^{17}\Delta$. For instance, Wurgaft

325 et al. (2013) showed from 700 m deep profiles in the Gulf of Elat that the $^{17}\Delta$ below the thermocline varied considerably with seasons, which they related to vertical as well as horizontal mixing. In order to evaluate the behaviour of $^{17}\Delta$ in the deep water of SCS Sea and its potential utility as a novel tracer, in an oceanographically very distinct system, we measured for the first time the $^{17}\Delta$ composition of deep O_2 profiles (down to 3500 m depth) from SEATS.

330 An overview of the oceanography of SCS is available in Wong et al. (2007). The subsurface water masses in SCS consist of three main water masses; 1) the Tropical Water situated at around 150 m originating from near the international dateline at 20–30 °N in the North Pacific (Suga et al., 2003), 2) the North Pacific Intermediate Water centred around 500 m with a source in the subpolar regions in the North Pacific (You, 2003), and 3) the Deep Water below 2200 m. The Deep Water in the SCS basin is formed by Pacific water masses, which in the western Philippine Sea overflow the sill that separates it from

335 the SCS. The characteristics of the deep water are rather uniform and similar to those in the western Philippine Sea, maintained by a mass balance between the inflowing deep water from the Phillipine Sea, upwelling and mixing with the shallower North Pacific Intermediate Water, and outflow at an intermediate depth through the Luzon Strait (Gong et al, 1992; Chao et al., 1996b; Hu et al., 2000).

340 Our data show overall elevated $^{17}\Delta$ values (>140 per meg) below 200 m depth for both August 2014 and April 2015 profiles. Largest variations were found at 200 m with a decrease of 116 per meg from August 2014 to April 2015 (Fig. 5a), coinciding with changes in the temperature-salinity characteristics of the Tropical Water mass (Fig. 5b). The coeval decrease in $^{17}\Delta$ and increase in temperature-salinity at this depth illustrate the increased winter inflow of water to the SCS from Kuroshio through the Luzon Strait, or possibly also partially from the East China Sea through the Taiwan Strait (Fig. 1). This

345 highlights the importance of NEM winds on driving the seasonal circulation inducing vertical mixing, which extends down to 400 m and leads to a full exchange of water masses during a winter (Fig. 5a). Historic records also support intrusions of North Pacific water masses to the South China Sea all year around with greatest strength in winter (Qu et al., 2000). Below, the deeper water remained relatively homogenous, and did not appear to be influenced by seasonal changes, marking the limit of the extent of monsoon-driven circulation influence on the mixing. Surprisingly, variations in $^{17}\Delta$ (around ~20 per

350 meg) were found beneath the thermocline base, however, considering the low O_2 content at these depths, even very minor changes in O_2 may result in a large effect on the $^{17}\Delta$ signal, and thus their interpretation should be taken with caution. Although further observations from the SCS are needed for a more comprehensive picture, our first results advocate for the

$^{17}\Delta$ as a valuable tracer of mixing processes, which brings new insights into some of the key aspects of our understanding of the circulation in SCS.

5 Conclusions

In summary, this study provides first insights into the $^{17}\Delta$ composition of dissolved O_2 at the SEATS station and within the SCS. We find the coupled $^{17}\Delta$ and $\Delta(O_2/Ar)$ approach a useful tracer, enabling us to monitor the seasonal changes in atmospheric vs. photosynthetic O_2 input in the upper part of the ocean. Our results show that the net biological O_2 production is highest during the winter, closely dependent on the northeast monsoon forcing, which intensity appears to dictate the sufficiency of the ecosystem to shift to net autotrophy. Moreover, we find the $^{17}\Delta$ of the deep water a promising novel tracer for mixing process, permitting us to evaluate the extent of the basin-wide monsoon-driven circulation in the water column and at depth, as well as revisit the deep mixing processes. Although further work is required before the deep $^{17}\Delta$ may be confidently applied as a conservative tracer of water mass mixing, our study shows that it could bring new perspectives on the renewal rate of deep water, at least within the South China Sea, and thus further deep $^{17}\Delta$ measurements within the region but also globally would be desirable. Lastly, we would like to encourage future studies considering increased spatio-temporal resolution of upper water $^{17}\Delta$ measurements within the SCS, which will be critical for gaining a more comprehensive picture into the primary productivity dynamics in the SCS and its responses to monsoon and/ or anthropogenic influences.

Data availability

The geochemical data used in this study are available in the Supplement accompanying this contribution. CTD data are available upon request.

Acknowledgements

This work was in part supported by a Ministry of Science and Technology (MOST), Taiwan grant 108-2111-M-001-011-MY3 to Academia Sinica, and Academia Sinica Investigator Award AS-IA-109-M03. Support from Taiwan's R/V Ocean Researcher-1 and the crew members is gratefully acknowledged.

References

Barkan E. and Luz B.: High-precision measurements of $^{17}O/^{16}O$ and $^{18}O/^{16}O$ of O_2 and O_2/Ar ratio in air. Rapid Communication in Mass Spectrometry 17, 2809–2814, https://doi.org/10.1002/rcm.1267, 2003.

Benson B. B. and Krause Jr. D. K.: The concentration and isotopic fractionation of oxygen dissolved in freshwater and
380 seawater in equilibrium with the atmosphere. Limnology and Oceanography 29, 620–632,
https://doi.org/10.4319/lo.1984.29.3.0620, 1984.

Cai W.-J. and Dai M.: Comment on ''Enhanced open ocean storage of CO_2 from shelf sea pumping''. Science 306, 1477,
https://doi.org/10.1126/science.1102132, 2004.
385

Castro-Morales K., Cassar N., Shoosmith D. R., and Kaiser J.: Biological production in the Bellingshausen Sea from
oxygen-to-argon ratios and oxygen triple isotopes. Biogeosciences 10, 2273–2291, https://doi.org/10.5194/bg-10-2273-2013,
2013.

390 Chao S.-Y., Shaw P.-T., Wu S.S.: El Niño modulation of the South China Sea circulation. Progress in Oceanography 38, 51–
93, https://doi.org/10.1016/S0079-6611(96)00010-9, 1996a.

Chao S.-Y., Shaw P.-T., Wu S.S.: Deep water ventilation in the South China Sea. Deep-Sea Research I 43, 445–466,
https://doi.org/10.1016/0967-0637(96)00025-8, 1996b.
395

Chen C.-T. A., Liu K.-K.., Macdonald R.: Continental margin exchanges, in Ocean Biogeochemistry: The Role of the Ocean
Carbon Cycle in Global Change. Edited by M. J. R. Fasham, Springer, New York, 53–98, https://doi.org/10.1007/978-3-642-
55844-3_4, 2003.

400 Chen, Y. L.: Spatial and seasonal variations of nitrate-based new production and primary production in the South China Sea.
Deep-Sea Research I 52, 319–340, https://doi.org/10.1016/j.dsr.2004.11.001, 2005.

Carr M.-E., et al.: A comparison of global estimates of marine primary production from ocean color. Deep-Sea Research II
53, 741–770, https://doi.org/10.1016/j.dsr2.2006.01.028, 2006.
405

Duce R.A., et al. The atmospheric input of trace species to the world ocean. Global Biogeochemical Cycles 5, 193–259,
https://doi.org/10.1029/91GB01778, 1991.

DeGrandpre M.D., Olbu G.J., Beatty C.M., Hammar T.R.: Air-CO_2 fluxes on the US Middle Atlantic Bight. Deep Sea
410 Research Part II: Topical Studies in Oceanography 49, 4355–4367, https://doi.org/10.1016/S0967-0645(02)00122-4, 2002.

Emerson S., Quay P. D., Stump C., Wilbur D., and Schudlich R.: Chemical tracers of productivity and respiration in the subtropical Pacific Ocean. Journal of Geophysical Research: Oceans 100, 15873–15887, https://doi.org/10.1029/95JC01333, 1995.

415

Frankignoulle M. and Borges A.V.: European continental shelf as a significant sink for atmospheric carbon dioxide. Global Biogeochemical Cycles 15, 569–576, https://doi.org/10.1029/2000GB001307, 2001.

Fung I.Y., Meyn S.K., Tegen I., Doney S.C., John J.G., Bishop J.K.B.: Iron supply and demand in the upper ocean. Global
420   Biogeochemical Cycle 14, 281–296, https://doi.org/10.1029/1999GB900059, 2000.

Gong G.-C., Liu K.K., Liu C.-T., and Pai S.-C.: The chemical hydrography of the South China Sea west of Luzon and a comparison with the West Philippine Sea. TAO 3, 587-602, https://doi.org/10.3319/TAO.1992.3.4.587(O), 1992.

425   Hamme R. C., Cassar N., Lance V. P., Vaillancourt R. D., Bender M. L., Strutton P. G., Moore T. S., DeGrandpre M. D., Sabine C. L., Ho D. T., and Hargreaves B. R.: Dissolved O_2/Ar and other methods reveal rapid changes in productivity during a Lagrangian experiment in the Southern Ocean. Journal of Geophysical Research 117, C00F12, https://doi.org/10.1029/2011JC007046, 2012.

430   Hendricks M.B., Bender M.L., Barnett B.A.: Net and gross O_2 production in the Southern Ocean from measurements of biological O_2 saturation and its triple isotope composition. Deep Sea Research Part I: Oceanographic Research Papers 51, https://doi.org/10.1016/j.dsr.2004.06.006, 1541–1561, 2004.

Hu J., Kawamura H., Hong H., and Qi Y.: A Review on the Currents in the South China Sea: Seasonal Circulation, South
435   China Sea Warm Current and Kuroshio Intrusion. Journal of Oceanography 56, 607–624, https://doi.org/10.1023/A:1011117531252, 2000.

Ho D.T., Law C.S., Smith M.J., Schlosser P., Harvey M., and Hill P.: Measurements of air-sea gas exchange at high wind speeds in the Southern Ocean: Implications for global parametrizations. Geophysical Research Letters 33, L16611,
440   https://doi.org/10.1029/2006GL026817, 2006.

Hsu H.-H. and Chen C.-T.: Observed and projected climate change in Taiwan. Meteorology and Atmospheric Physics 79, 87–104, https://doi.org/10.1007/s703-002-8230-x, 2002.

445   Juranek L.W. and Quay P.D.: In vitro and in situ gross primary and net community production in the North Pacific Subtropical Gyre using labelled and natural abundance isotopes of dissolved O_2. Global Biogeochemical Cycles 19, GB30009, https://doi.org/10.1029/2004GB002384, 2005.

Juranek L. W. and Quay P. D.: Using triple isotopes of dissolved oxygen to evaluate global marine productivity. Annual
450   Review of Marine Science 5, 503–524, https://doi.org/10.1146/annurev-marine-121211-172430, 2013.

Juranek L. W., Quay P. D., Feely R. A., Lockwood D., Karl D. M., and Church M. J.: Biological production in the NE Pacific and its influence on air-sea CO_2 flux: Evidence from dissolved oxygen isotopes and O_2/Ar. Journal of Geophysical Research 117, C05043, https://doi.org/10.1029/2011JC007450, 2012.
455

Jurikova H., Guha T., Abe O., Shiah F.-K., Wang C.-H., and Liang M.-C.: Variations in triple isotope composition of dissolved oxygen and primary production in a subtropical reservoir. Biogeosciences 13, 6683–6698, https://doi.org/10.5194/bg-13-6683-2016, 2016.

460   Kaiser J., Reuer M. K., Barnett B., and Bender M. L.: Marine productivity estimates from O_2/Ar ratio measurements by membrane inlet mass spectrometry. Journal of Geophysical Research 32, L19605, https://doi.org/10.1029/2005GL023459, 2005.

Kaiser J.: Technical note: Consistent calculation of aquatic gross production from oxygen triple isotope measurements.
465   Biogeosciences 8, 1793–1811, https://doi.org/10.5194/bg-8-1793-2011, 2011.

Karl D.M. and Lukas R.: The Hawaii Ocean Time-series (HOT) program: Background, rationale and field implementation. Deep Sea Research Part II: Topical Studies in Oceanography 43, 129–156, https://doi.org/10.1016/0967-0645(96)00005-7, 1996.
470

Laws E. A.: Photosynthetic quotients, new production and net community production in the open ocean. Deep-Sea Research I 38, 143– 167, https://doi.org/10.1016/0198-0149(91)90059-O, 1991.

Laws E. A., Landry M. R., Barber, R. T., Campbell L., Dickson M. L., and Marra J.: Carbon cycling in primary production
475   bottle incubations: inferences from grazing experiments and photosynthetic studies using ^{14}C and [18]O in the Arabian Sea. Deep-Sea Res. II, 47, 1339–1352, https://doi.org/10.1016/S0967-6645(99)00146-0, 2000.

Li H., Wiesner M.G., Chen J., Ling Z., Zhang J., Ran L.: Long-term variation of mesopelagic biogenic flux in the central South China Sea: Impact of monsoonal seasonality and mesoscale eddy. Deep-Sea Research Part I 126, 62−72, 480 https://doi.org/10.1016/j.dsr.2017.05.012, 2017.

Lin I.-I., Chen J.-P., Wong G.T.F., Huang C.-W., Lien C.-C.: Aerosol input to the South China Sea: Results from the MODerate Resolution Imaging Spectro-radiometer, the quick Scatterometer, and the Measurements of Pollution in the Troposphere Sensor. Deep-Sea Research Part II 54, 1589−1601, https://doi.org/10.1016/j.dsr2.2007.05.013, 2007.

485

Liang M.-C. and Mahata S. (2015) Oxygen anomaly in near surface carbon dioxide reveals deep stratospheric intrusion. Scientific Reports 5, 11352, https://doi.org/10.1038/srep11352, 2015.

Liang M.-C., Mahata S., Laskar A.H., Thiemens M.H., and Newman S.: Oxygen isotope anomaly in tropospheric CO_2 and 490 implications for CO_2 residence time in the atmosphere and gross primary productivity. Scientific Reports 7, https://doi.org/10.1038/s41598-017-12774-w, 2017.

Liu K.-K., Atkinson L., Chen C.T.A., Gao S., Hall J., MacDonald R.W., McManus L.T., Quiñones R.: Exploring continental margin carbon fluxes on a global scale. EOS 81, 641–644, . https://doi.org/10.1029/EO081i052p00641-01, 2000.

495

Liu K.-K., Chao S.-Y., Shaw P.T., Gong G.-C., Chen C.-C., Tang T.Y.: Monsoon-forced chlorophyll distribution and primary production in the South China Sea: observations and a numerical study. Deep-Sea Research Part I 49, 1387−1412, https://doi.org/10.1016/S0967-0637(02)00035-3, 2002.

500 Luz B. and Barkan E.: Assessment of Oceanic Productivity with the Triple-Isotope Composition of Dissolved Oxygen. Science 288, 2028–2031, https://doi.org/ 10.1126/science.288.5473.2028, 2000.

Luz B. and Barkan E.: The isotopic ratios $^{17}O/^{16}O$ and $^{18}O/^{16}O$ in molecular oxygen and their significance in biogeochemistry. Geochimica et Cosmochimica Acta 69, 1099–1110, https://doi.org/10.1016/j.gca.2004.09.001, 2005.

505

Luz B., Barkan E., Bender M. L., Thiemens M. H., and Boering K. A.: Triple-isotope composition of atmospheric oxygen as a tracer of biosphere productivity. Nature 400, 547–550, https://doi.org/10.1038/22987, 1999.

Luz B., Barkan E., Sagi Y., and Yacobi Y. Z.: Evaluation of community respiratory mechanisms with oxygen isotopes: A 510 case study in Lake Kinneret. Limnology and Oceanography 47, 33–42, https://doi.org/10.4319/lo.2002.47.1.0033, 2002.

Luz B., and Barkan E.: Proper estimation of marine gross O_2 production with $^{17}O/^{16}O$ and $^{18}O/^{16}O$ ratios of dissolved O_2. Geophysical Research Letters 38, L19606, https://doi.org/10.1029/2011GL049138, 2011.

515   Marra J.: Approaches to the measurement of plankton production, Phytoplankton productivity: carbon assimilation in marine and freshwater ecosystem. Edited by Willams P. J. le B., Thomas D. N., and Reynolds C. S. Cambridge, Blackwells, 78–108, https://doi.org/10.1002/9780470995204.ch4, 2002.

Ning X., Chai F., Xue H., Cai Y., Liu C., and Shi J.: Physical-biological oceanographic coupling influencing phytoplankton
520   and primary production in the South China Sea. Journal of Geophysical Research 1009, C10005, https://doi.org/10.1029/2004JC002365, 2004.

Pai S. C., Gong G. C., and Liu K. K.: Determination of dissolved oxygen in seawater by direct spectrophotometry of total iodine. Marine Chemistry 41, 343–351, https://doi.org/10.1016/0304-4203(93)90266-Q, 1993.

525

Prokopenko M. G., Pauluis O. M., Granger J., and Yeung L. Y.: Exact evaluation of gross photosynthetic production from the oxygen triple-isotope composition of O_2: Implications for the net-to-gross primary production ratios. Geophysical Research Letters 38, L14603, https://doi.org/10.1029/2011GL047652, 2011.

530   Qu T., Mitsudera H., Yamagata T.: Intrusion of the North Pacific waters into the South China Sea. Journal of Geophysical Research 105, 6415–6424, https://doi.org/10.1029/1999JC900323, 2000.

Quay P.D., Peacock C., Björkman K., Karl D.M.: Measuring primary production rates in the ocean: Enigmatic results between incubation and non-incubation methods at Station ALOHA. Global Biogeochemical Cycles 24, GB3014,
535   https://doi.org/10.1029/2009GB003665, 2010.

Regaudie-de-Gioux A., Lasternas S., Augustí S., and Duarte C.M.: Comparing marine primary production estimates through different methods and development of conversion equations. Frontiers in Marine Science 1, 19, https://doi.org/10.3389/fmars.2014.00019, 2014.
540

Rehder G. and Suess E.: Methane and pCO$_2$ in the Kuroshio and the South China Sea during maximum summer surface temperatures. Marine Chemistry 75, 89–108, https://doi.org/10.1016/S0304-4203(01)00026-3, 2001.

Reuer M.K., Barnett B.A., Bender M.L., Falkowski P.G., Hendricks M.B.: New estimates of Southern Ocean biological
545   production rates from O_2/Ar ratios and the triple isotope composition of O_2. Deep Sea Research I 54, 951–974,
https://doi.org/10.1016/j.dsr.2007.02.007, 2007.

Sarma V. V. S. S., Abe O., Hashimoto S., Hinuma A., and Saino T.: Seasonal variations in triple oxygen isotopes and gross
oxygen production in the Sagami Bay, central Japan. Limnology and Oceanography 50, 544–552,
550   https://doi.org/10.4319/lo.2005.50.2.0544, 2005.

Seguro I., Marca A.D., Painting S.J., Shutler J., Suggett D.J., and Kaiser J.: High-resolution net and gross biological
production during a Celtic Sea spring bloom. Progress in Oceanography 177, 101885,
https://doi.org/10.1016/j.pocean.2017.12.00, 2019.
555
Schlitzer R.: Ocean Data View, https://odv.awi.de/, 2020.

Stanley R. H. R., Kirkpatrick J. B., Cassar N., Barnett B. A., and Bender M. L.: Net community production and gross
primary production rates in the western equatorial Pacific. Global Biogeochemical Cycles 24, GB4001,
560   https://doi.org/10.1029/2009GB003651, 2010.

Steeman-Nielsen E.: The use of radioactive carbon (^{14}C) for measuring organic production in the sea. ICES Journal of
Marine Science (Journal du Conseil) 18, 117–140, https://doi.org/10.1093/icesjms/18.2.117, 1952.

565   Suga T., Kato A., Hanawa K.: North Pacific Tropical Water: its climatology and temporal changes associated with the
climate regime shift in the 1970s. Progress in Oceanography 47, 223–256, https://doi.org/10.1016/S0079-6611(00)00037-9,
2003.

Thomas H., Bozec Y., Elkalay K., de Baar H.J.W.: Enhanced Open Ocean Storage of CO_2 from Shelf Sea Pumping. Science
570   304, 1005–1008, https://doi.org/10.1126/science.1095491, 2004.

Tseng C.-M., Wong G.T.F., Lin I.-I., Wu C.-R., and Liu K.-K.: A unique seasonal pattern in phytoplankton biomass in low-
latitude waters in the South China Sea. Geophysical Research Letters 32, L08608, https://doi.org/10.1029/2004GL022111,
2005.
575
Tsunogai S., Watanabe S., and Sato T.: Is there a "continental shelf pump" for the absorption of atmospheric CO_2? Tellus 51,
701−712, https://doi.org/10.1034/j.1600-0889.1999.t01-2-00010.x, 1999.

Wang S.-L., Chen C.-T.A., Hong G.-H., and Chung C.-S.: Carbon dioxide related parameters in the East China Sea.
580   Continental Shelf Research 2000, 525–544, https://doi.org/10.1016/S0278-4343(99)00084-9, 2000.

Wanninkhof R., Asher W. E., Ho D. T., Sweeney C., and McGillis W. R.: Advances in quantifying air-sea gas exchange and
environmental   forcing.   Annual   Review   of   Marine   Science   1,   213–244,
https://doi.org/10.1146/annurev.marine.010908.163742, 2009.

585

Wong G.T.F., Ku T.-L., Mulholland M., Tseng C.M., and Wang D.-P.: The SouthEast Asian Time-series Study (SEATS)
and the biogeochemistry of the South China Sea – An overview. Deep-Sea Research Part II 54, 1434−1447,
https://doi.org/10.1016/j.dsr2.2007.05.012, 2007.

590   Wurgaft E., Shamir O., Barkan E., Paldor N., and Luz B.: Mixing processes in the deep water of the Gulf of Elat (Aqaba):
evidence from measurements and modelling of the triple isotopic composition of dissolved oxygen. Limnology and
Oceanography 58, 1373−1386, https://doi.org/10.4319/lo.2013.58.4.1373, 2013.

Xu M., Chang C.-P., Fu C., Qi Y., Robock A., Robinson D., and Zhang H.-M.: Steady decline of east Asian monsoon winds,
595   1969–2000: Evidence from direct ground measurements of wind speed. Journal of Geophysical Research 111, D24111,
https://doi.org/10.1029/2006JD00733, 2006.

Yool A. and Fasham M.J.R.: An examination of the "Continental shelf pump" in an open ocean general circulation model.
Global Biogeochemical Cycles 15, 831–844, https://doi.org/10.1029/2000GB001359, 2001.

600

You Y.: The pathway and circulation of North Pacific Intermediate Water. Geophysical Research Letters 30, 2291,
https://doi.org/10.1029/2003GL018561, 2003.

Zhai W., Dai M., Cai W.-J., Wang Y., Hong H.: The partial pressure of carbon dioxide and air-sea fluxes in the northern
605   South   China   Sea   in   spring,   summer   and   autumn.   Marine   Chemistry   96,   87–97,
https://doi.org/10.1016/j.marchem.2004.12.002, 2005.

Date	PLD[a]	MLD[b]	C_o	K from U	$\Delta(O_2/Ar)$	$^{17}\Delta$	NP	GP	NCP /
	(m)	(m)	(mmol m^{-3})	(m d^{-1})	(%)	(per meg)			GCP
Oct. 16th, 2013	81	49	201.29	3.1	−	123	−	5895	−
Aug. 5th, 2014	77	31	198.04	3.6	−0.5	59	−29	1830	−0.02
Aug. 6th, 2014	79	31	198.04	3.6	−0.2	57	−15	1761	−0.01
Apr. 24th, 2015	101	23	204.63	4.6	−2	57	−160	2311	−0.07
Apr. 25th, 2015	101	23	204.63	4.6	1.9	28	152	721	0.21

[a] Photic layer depth. [b] Mixed layer depth.

Table 1: Mixed-layer integrated dissolved oxygen composition, and estimated seasonal primary production rates at the SouthEast Asian Time-series Study (station 55, "SEATS") in the South China Sea (SCS) for October 2013 (inter-monsoon period), August 2014 (SWM) and April 2015 (NEM). Both, NP and GP are in mg C m−2 d−1. Note that these production estimates present rather an underestimate as some production has also likely taken place below the mixed layer.
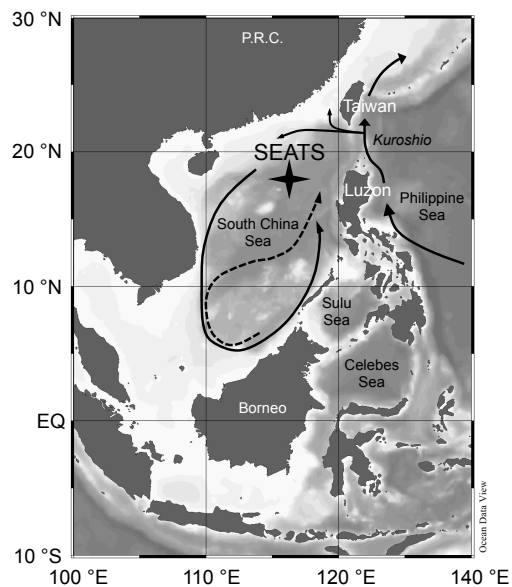
Figure 1: Bathymetric map of South China Sea (SCS) and surrounding areas with position of The SouthEast Asian Time-series Study (station 55, "SEATS") indicated. Arrows in SCS indicate the circulation patterns – solid line shows the basin-wide cyclonic gyre during winter, dashed line represents the eastward jet off the Vietnam coast and the anticyclonic gyre over the southern half of SCS throughout the summer. Map was created using Ocean Data View (https://odv.awi.de/; Schlitzer, 2020).
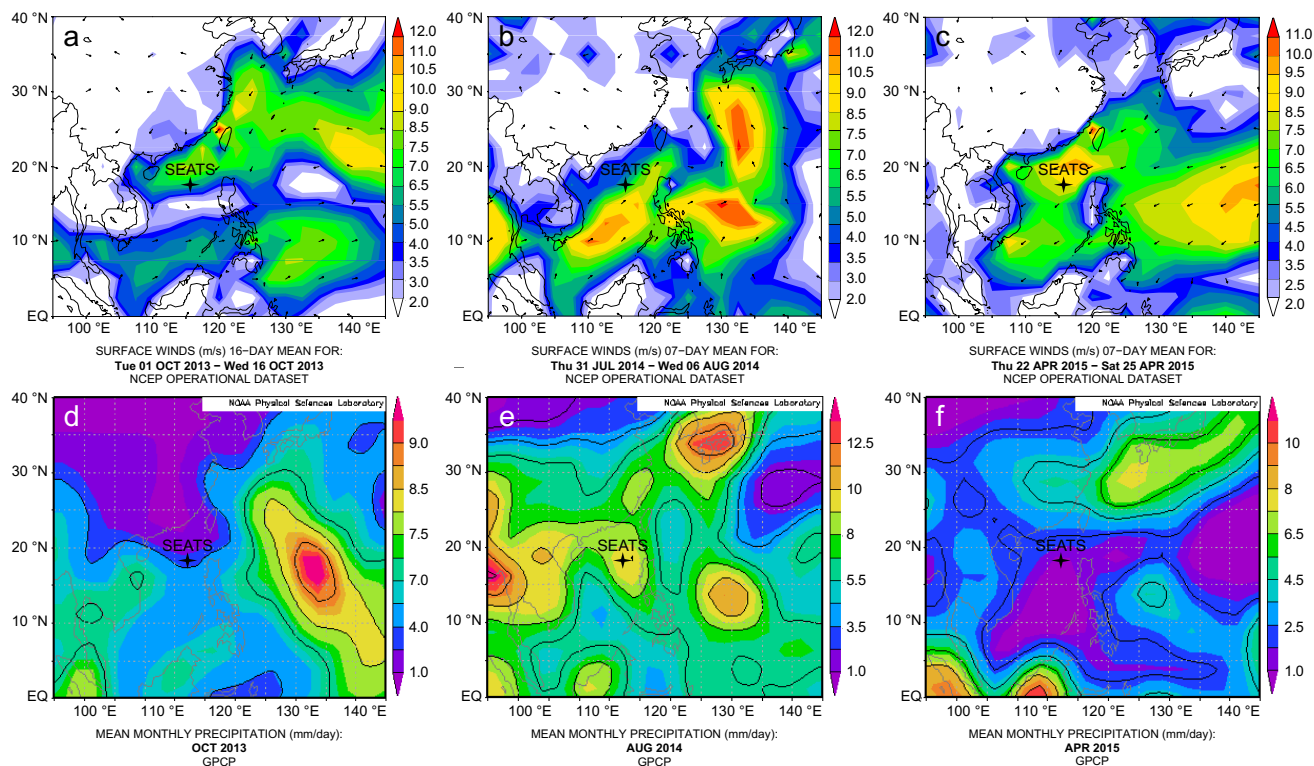
Figure 2: Upper panels – surface vector wind maps indicating the monsoon seasons: a) inter-monsoon period in October 2013; b) southwest summer monsoon in August 2014; c) northeast winter monsoon in April 2015. Lower panels – mean monthly precipitation: d) in October 2013; e) in August 2014; c) and in April 2015. Maps of vector winds distributions were obtained from the NOAA – Atmospheric Variables Plotting Page using the NCEP daily analysis data (https://www.esrl.noaa.gov/psd/data/histdata/). Maps of precipitation were obtained from NOAA's GPCP Version 2.3 Combined Precipitation Data Set (https://psl.noaa.gov/data/gridded/data.gpcp.html).

620
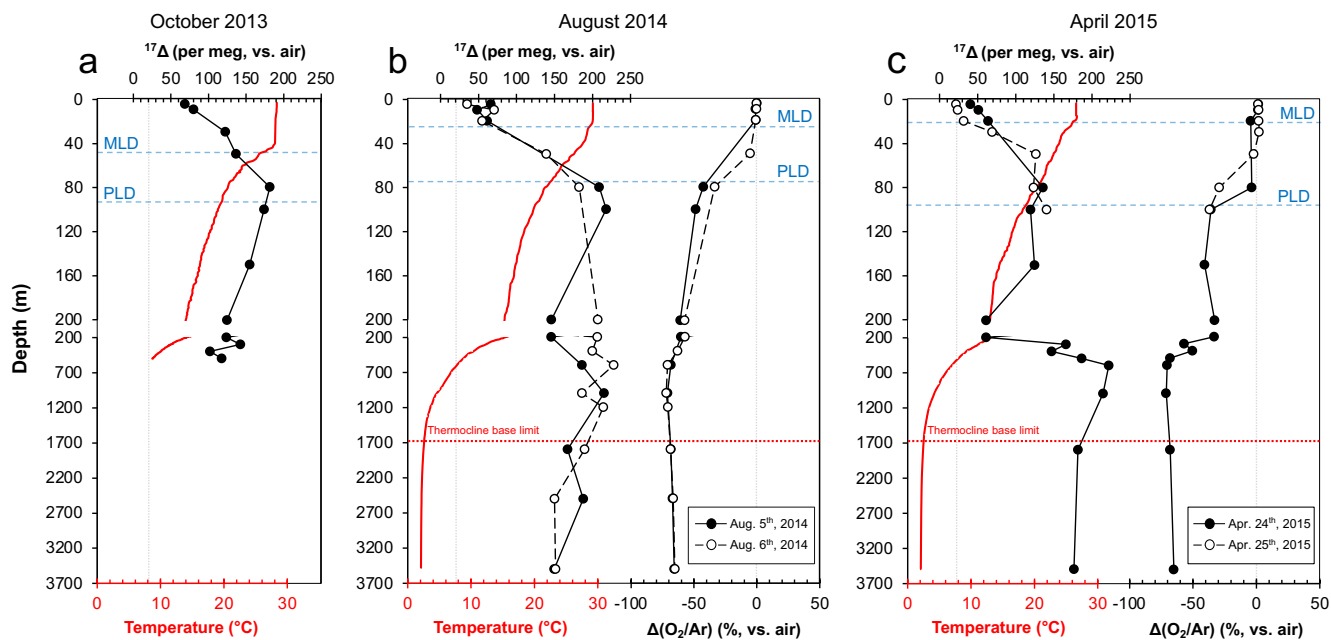
Figure 3: Depth profiles of temperature (red lines) and $^{17}\Delta$ and $\Delta(O_2/Ar)$ profiles (solid or dashed black lines) from SEATS during: a) inter-monsoon seasons; b) summer southwest (SWM); and c) winter northeast monsoon (NEM). Vertical dashed grey lines indicate the equilibrium $^{17}\Delta$ and $\Delta(O_2/Ar)$ values with atmosphere. MLD−mixed layer depth, PLD−photic layer depth.
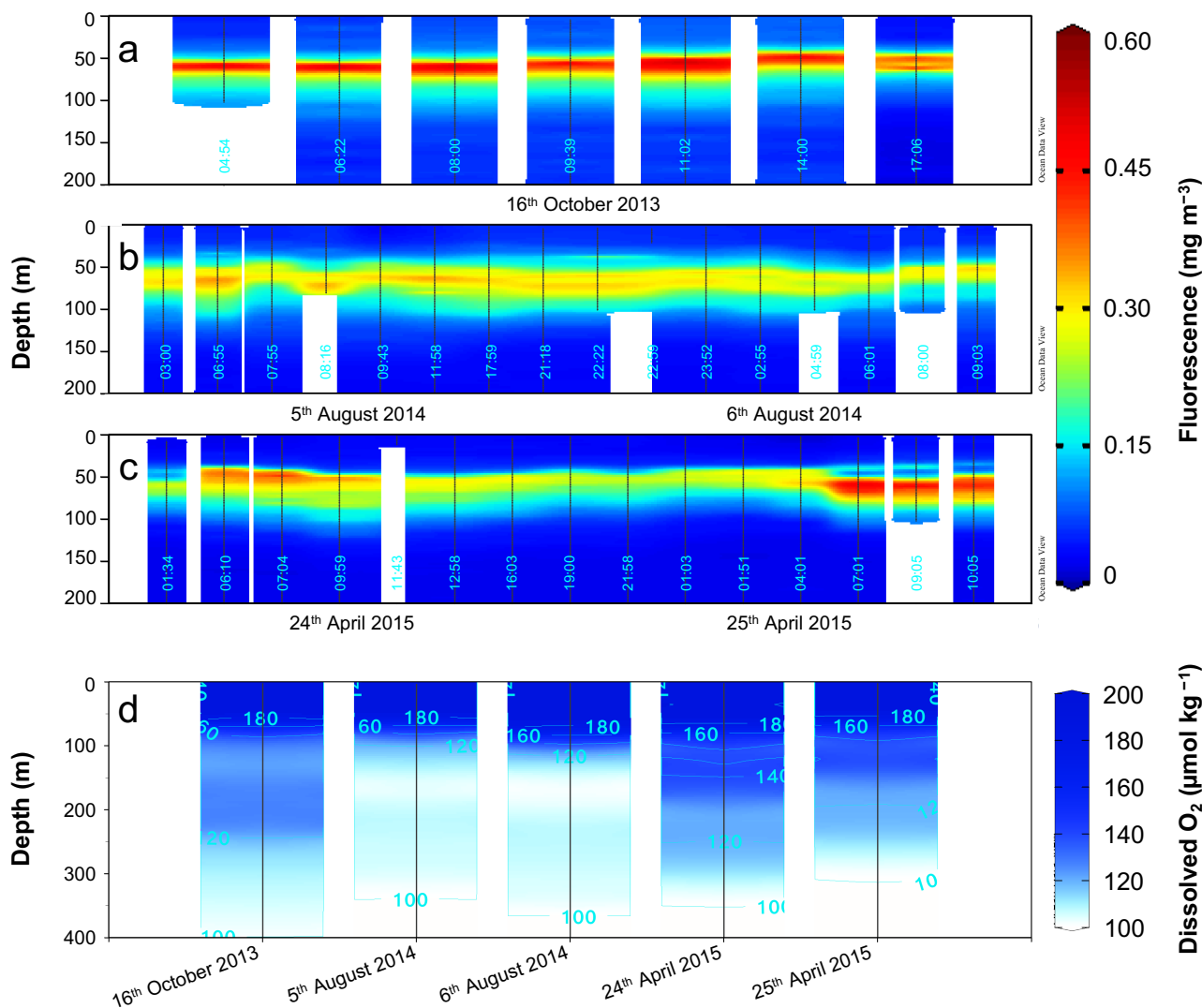
Figure 4: Depth profiles of fluorescence (mg m⁻³) time-series from SEATS: a) inter-monsoon period (16th October 2013); b) summer southwest (SWM; 5th–6th August 2014); and c) winter northeast monsoon (NEM; 24th–25th April 2015); and dissolved oxygen concentration (μmol kg⁻¹) in the upper water column on the different sampling days. Maps were created using Ocean Data View (https://odv.awi.de/; Schlitzer, 2020).
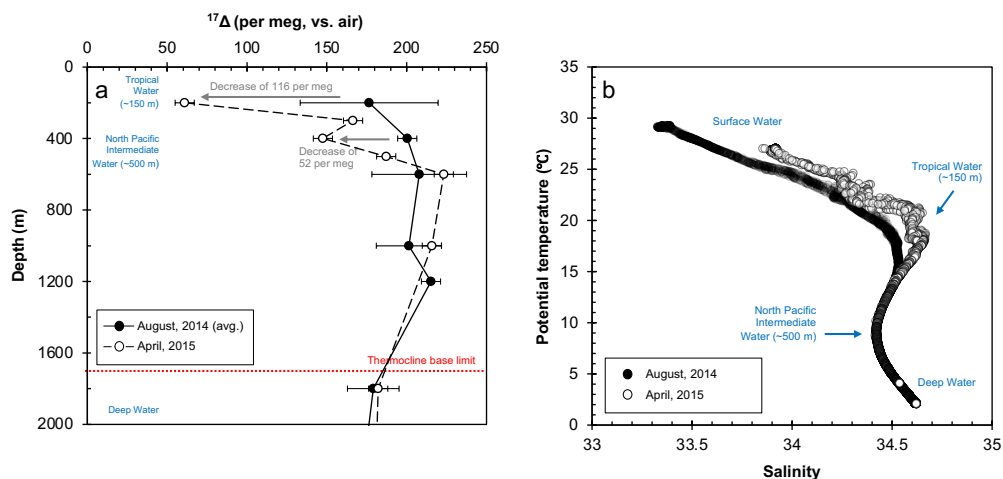
Figure 5: Deep water composition at SEATS from August 2014 to April 2015; a) $^{17}\Delta$ of dissolved O$_2$. Error bars indicate the standard deviation between duplicates (1σ) where available or the analytical uncertainty (6 per meg; 1σ) The $^{17}\Delta$ values from August 2014 are presented as mean of the two sampling days (5th and 6th). b) relationship between potential temperature and salinity. Salinity peak of ~34.6 (and ~20 °C) corresponds to the Tropical Water situated around 150 m, while the minimum of ~34.4 indicates the North Pacific Intermediate at around 500 m. The Deep Water below the thermocline base (~1700 m) is characterised by low temperatures ~2 °C and high salinities around ~34.6.